

A three-dimensional, anatomically detailed foot model: A foundation for a finite element simulation and means of quantifying foot-bone position

Daniel L.A. Camacho, MD, PhD; William R. Ledoux, PhD; Eric S. Rohr, MS; Bruce J. Sangeorzan, MD; Randal P. Ching, PhD

Department of Veterans Affairs Rehabilitation Research and Development Center for Excellence in Limb Loss Prevention and Prosthetic Engineering, Seattle, WA 98108; Department of Orthopaedics and Sports Medicine, University of Washington, Seattle, WA 98195

Abstract—We generated an anatomically detailed, three-dimensional (3-D) reconstruction of a human foot from 286 computerized topographic (CT) images. For each bone, 2-D cross-sectional data were obtained and aligned to form a stacked image model. We calculated the inertial matrix of each bone from the stacked image model and used it to determine the principal axes. Relative angles between the principal axes of the bones were employed to describe the shape of the foot, i.e., the relationships between the bones of the foot. A 3-D surface model was generated from the stacked image models and a detailed 3-D mesh for each bone was created. Additionally, the representative geometry of the plantar soft tissue was obtained from the CT scans, while the geometries of the cartilage between bones were obtained from the 3-D surface bone models. This model served dual purposes: it formed the anatomical foundation for a future finite element model of the human foot and we used it to objectively quantify foot shape using the relationships between the principal axes of the foot bones.

Key words: *anatomic models, computerized topography, computer models, foot, structural models.*

INTRODUCTION

Increasingly, musculoskeletal models of the human body are used as powerful tools to study biological structures; however, they frequently lack the geometric detail necessary to provide meaningful insights into biomechanical behavior. The lower limb, and in particular the foot, is of interest because it is the primary physical interaction between the body and the environment during locomotion. Just how variations in foot structure affect the interaction between the body and the environment is an ongoing research question. The work of Morag and Cavanagh has demonstrated that foot structure, as determined by two-dimensional (2-D) X-ray measurements, can affect plantar pressure [1]. Objective measure of the 3-D relationships of the bones, rather than 2-D angular projections to cardinal planes, may provide further insight into foot-bone architecture.

Simplified biomechanical models of the foot have been generated but have lacked the necessary detail to accurately model biomechanical behavior. Phenomenological foot models have not provided anatomically

This material is based on work supported by the Department of Veterans Affairs, Veterans Health Administration, Rehabilitation Research and Development Service, project number A0806C.

Address all correspondence and requests for reprints to William R. Ledoux, PhD, VA Puget Sound, MS 151, 1660 S. Columbian Way, Seattle, WA 98108; 206-768-5347, fax: 206-277-3963, email: wrledoux@u.washington.edu.

detailed information about the structures within the foot [2,3]. Others have developed models with better anatomical accuracy, including 2-D finite element models, but still lacked the detail required to study the individual motions of the bones of the foot [4–10].

Several 3-D finite element models of the human foot have been developed, but most have been uniquely tailored to study the loading that a lower limb may undergo in automobile accidents [11–15], while others have studied the effects of Hansen's disease [16]. These simulations range in fidelity and scope. The work of Beillas et al. is the most anatomically detailed model to date; it included osseous geometry obtained from computerized tomographic (CT) images, an approximation of cartilage geometry, foot and ankle ligaments, and plantar soft tissue properties [13]. However, the model did not include anatomical toes, the plantar soft tissue was modeled coarsely, and 3-D cartilage models were not included.

Another means of studying foot biomechanics, namely quantitative measures of foot shape (neutrally aligned, pes planus [low arch], and pes cavus [high arch]), are limited by subjective error. Footprint indexes have been developed to describe the relationship between the footprint and the height of the arch [17–21]. However, these measurements are 2-D descriptions of 3-D phenomena, have not been correlated with foot type, and involve potential rater error. Various radiographic parameters have been employed to quantify foot morphology [22–29] but a comprehensive study correlating foot type with X-ray parameters has not been performed. X-ray measurements are also 2-D descriptions of 3-D phenomena and are similarly limited by rater error. Static alignment devices have also been used to quantify the amount of medial malleolar displacement during quiet stance [30–33]. Although differences have been measured between foot types, the static alignment devices require that an operator place the device around a subject's limb and can only quantify rear foot position. Finally, CT images and the cardinal plane angular relationships between bones have been used to describe foot type [34]. However, the CT scans were not performed under weight-bearing conditions, measurements were only made in the two cardinal planes studied, and an observer was required to make the measurements, thus introducing further subjective error.

In summary, computational foot models have in general either lacked anatomical detail or been tailored for specific simulations. Further, all the aforementioned foot-

type determination parameters require input from an observer, which introduces a subjective component. The purpose of this research is twofold. First, this paper will describe the development of a 3-D, anatomically detailed model of the human foot from CT scans. This model will serve as the foundation for a future finite element model of the human foot. Second, the geometrical data of the bones will be used to generate objective 3-D descriptions of bone position. The relationships between bones will be used in the future as a way of describing differences between feet of different architectures. Data will be presented from one foot to demonstrate the two purposes.

METHODS

The CT images were acquired from the left cadaveric foot of a 67-year-old male donor. The specimen was obtained from the University of Washington Department of Biological Structure. No gross deformities or significant degenerative changes were evident on anteroposterior (AP) or lateral radiographs. To prepare the foot for scanning, we thawed the specimen, dissected away the soft tissue around the tibia, reamed the tibial intramedullary canal, and threaded an acrylic rod into the tibia. The specimen was supported with an acrylic frame within a Hi-Speed Advantage CT scanner (General Electric Medical Systems; Milwaukee, WI) (**Figure 1**). To hold the specimen in place, we loaded it with a nominal force

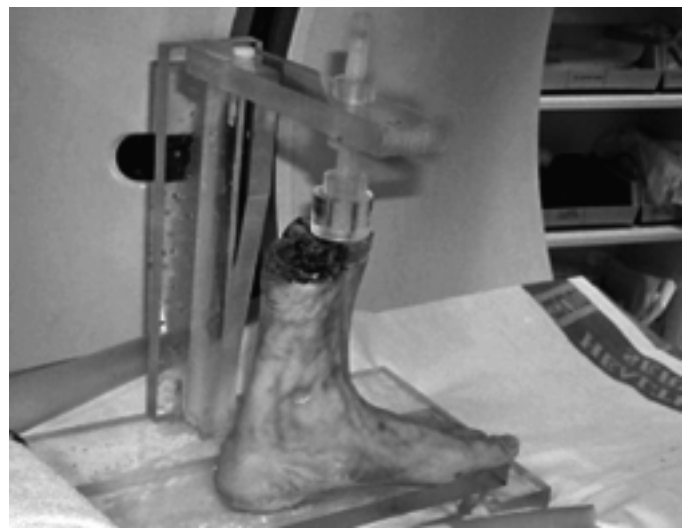


Figure 1. Cadaveric foot supported in acrylic loading frame in CT scanner.

within the frame. The threaded acrylic rod in the tibial shaft was cross-locked with an acrylic nut. The rod was held upright in the frame, and a second nut was used to apply minimal force to the foot and ankle with the tibia upright and the ankle at 90° , i.e., anatomical neutral position.

No attempt was made to load the foot to normal weight-bearing while it was being scanned. One future goal of this research is the development of a finite element foot model, which would require unloaded geometrical data to simulate initial conditions. Another future goal is the quantification of differences in foot architectures in live subjects, which would require that the feet be loaded before scanning. For our purposes, i.e., obtaining the geometric data for a future finite element model and demonstrating the use of principal axes to describe foot-bone position, non-weight-bearing data were deemed adequate.

Frontal plane CT images of the specimen were acquired at 1-mm intervals, beginning posteriorly with the heel and proceeding anteriorly to the toes. The scans were taken with 512×512 pixels over a $206\text{-mm} \times 206\text{-mm}$ area, for a dimensional accuracy of 0.4023 mm/pixel . For the entire foot to be scanned, 286 slices were required. We chose the frontal plane as the optimal scanning orientation because it avoided potential difficulties in data processing that can occur when a bone appears as multiple discontinuous regions in the same CT image.

Each bone was represented as a series of 2-D outlines from the CT images. The CT data were downloaded to a Macintosh G3 PowerPC workstation (Apple Computer, Inc.; Cupertino, CA) and visualized with the National Institutes of Health (NIH) Image 1.61 software (National Institutes of Health; Bethesda, MD). The 286 images were combined into a stack. For each slice, the contours outlining the cortical shell of a particular bone were derived with NIH Image's density slice option and automatic outlining tool (**Figure 2**). A threshold of 137 (on an 8-bit scale) was optimal for contrasting bone. In the rare instances that the border between two bones was suboptimally delineated with the automatic outlining tool, manual pixel-level user input was required to define the borders. Once the edge of the bone of interest was determined, the stack was advanced to the next slice and the process repeated until every slice containing the particular bone had been examined.

A custom segmentation macro for NIH Image (developed by Randal P. Ching) was created to obtain a

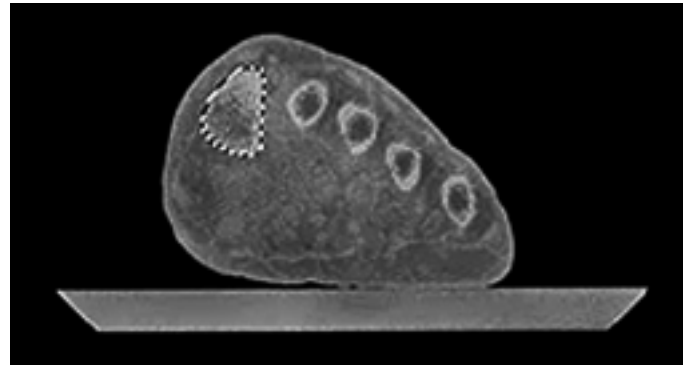


Figure 2.

A single CT slice with contour of first metatarsal cortical shell outlined.

description of the boundary of the object. The data, consisting of the x - y coordinates of each point that describe the shape of the boundary of each slice, was saved to a separate file. This process was repeated for all of the bones of the foot; the sesamoids were included with the first metatarsal.

A 3-D stacked image model for each bone was created from the 2-D data. Each bone was represented by a set of files describing each slice of the particular bone of interest. To combine the slices into one file as a stacked image model, a custom software program (PolyLines 1.9, developed by Randal P. Ching) was used. PolyLines sequentially read in each file of 2-D data (i.e., the x - y coordinates of the boundary of each slice) and combined the slices into a stacked image model by incorporating the space between slices as the global z -axis distance. To visualize the stacked image model, in the drawing exchange format (DXF), we converted the file to a Rotator file with a DXF-to-Rotator converter (<http://raru.adelaide.edu.au/rotater/>, developed by Craig Kloeden). The Rotator file was viewed with the Rotater 3.5 software package (<http://raru.adelaide.edu.au/rotater/>; developed by Craig Kloeden) (**Figure 3**). The stacked image model was examined from all sides to look for irregularities in the surface, with corrections (i.e., regenerating boundaries for a particular slice with NIH Image) made as necessary.

A 3-D surface model of each bone was generated from the stacked image model. Each bone's DXF file was imported into form•Z 3.5 (auto•des•sys, Inc., Columbus, OH), a 3-D form synthesizer, to create a 3-D surface model. The stacked image model served as control lines for the generation of a controlled mesh 3-D surface (**Figure 4**). A broken Bézier-controlled mesh-smoothing algorithm was used to generate the surface. All faces on

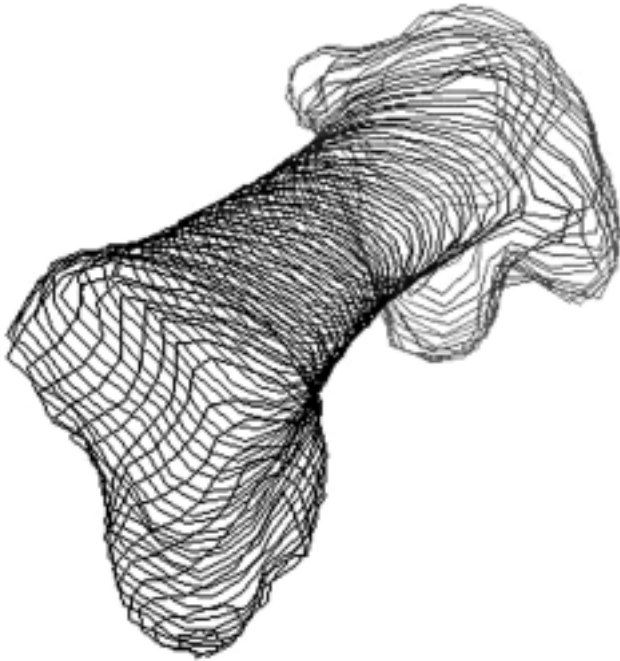


Figure 3.

A stacked image model of first metatarsal, demonstrating 2-D slices stacked together to form a 3-D object.

the surface were then triangulated. After the triangulated mesh was created, it was exported in stereolithography (STL) format.

A 3-D surface mesh of each bone, which will be a foundation for a finite element model, was created from the surface models. The final software package used in the model development process was TrueGrid 1.4 (XYZ Scientific Applications, Inc.; Livermore, CA), a finite element preprocessor and mesh generator. This software imported the 3-D STL file and enabled the mesh shape and density to be interactively generated by the user. The user selected the number of nodes as well as the initial position of the control nodes on the existing surface. The mesh was projected to the 3-D surface (**Figure 5**). The number of nodes was selected to produce a mesh that was sufficiently detailed to accurately model biomechanical behavior without being too detailed such that future finite element simulation times would be rendered intractable. As before, the bony image was rotated to identify defects in the generated mesh; if defects were found, the control nodes and the mesh density could be adjusted. Furthermore, several diagnostic measurements could be conducted on the mesh (e.g., the orthogonality and the



Figure 4.

3-D surface model of first metatarsal.

aspect ratio of each element) to quantify the quality of the mesh. A total of 7,022 four-noded shell elements were used to generate the surface mesh, ranging from 902 for the talus and 720 for the calcaneus to 32 for the fourth

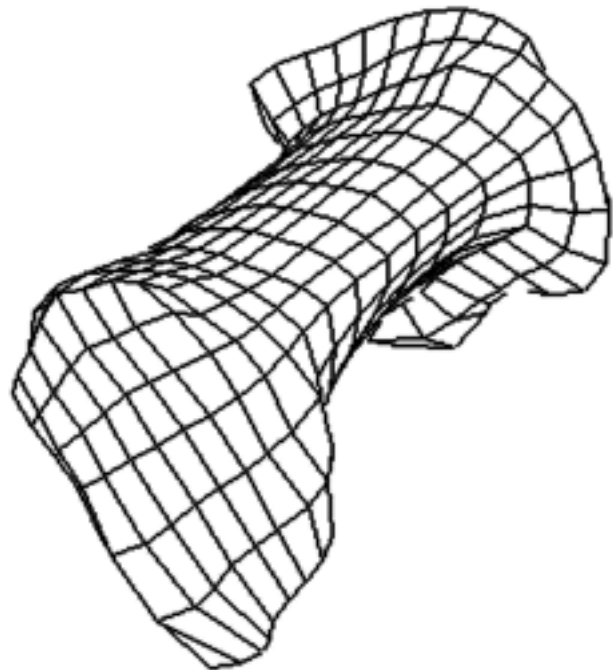


Figure 5.

Mesh representing surface geometry of first metatarsal.

distal phalange (**Figure 6**). We repeated this protocol for each of the bones of the foot. A mesh representative of the plantar soft tissue was also generated in this manner (**Figure 7**). The borders of these tissues included the dorsal aspect of the foot bones, as well as the medial, lateral, and dorsal aspects of the foot. The same procedures were employed, except for the threshold level in the NIH Image, which was adjusted to range from 133 to 185. The plantar soft tissue was represented by 2,112 eight-noded hexahedral elements.

The 3-D cartilage bodies were generated from the 3-D surface models of the bone, since the cartilage borders were not readily viewable in the CT scans. Once the bone models had been exported into form•Z, we generated representative cartilage bodies by creating a solid volume around the joint of interest. The bones were subtracted from the solid volume, and the remaining shape was trimmed to match the contours of the joint of interest (**Figure 8**). Note that separate layers of cartilage were not created for each bone; rather one 3-D object represented all of the cartilage between the two bones. As with the bony objects, the cartilage objects were saved in STL format and exported to TrueGrid for mesh generation. The meshes ranged from 47 eight-

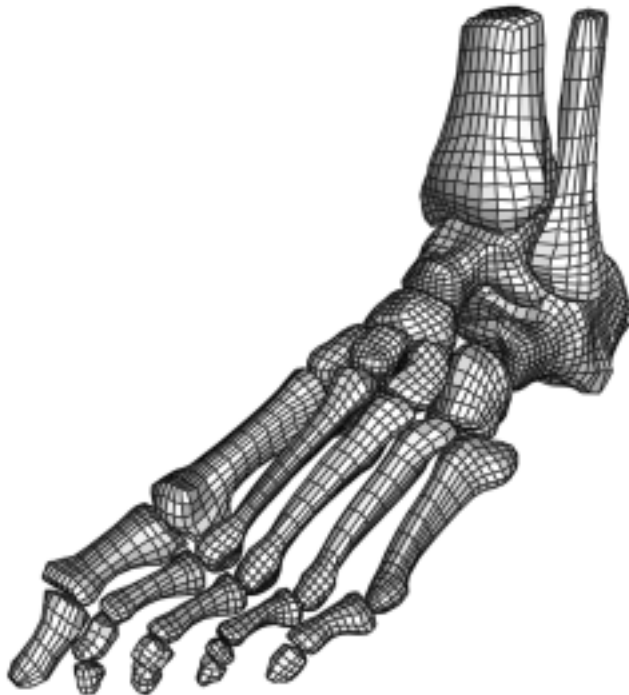


Figure 6.
Mesh representing surface geometry of all of bones of foot.

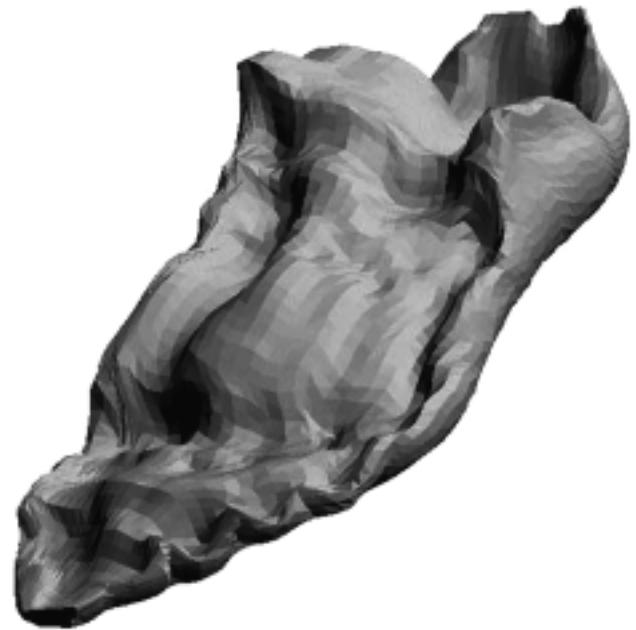


Figure 7.
3-D surface model representing plantar soft tissue.

noded hexahedral elements for the ankle-joint cartilage to nine elements for the calcaneocuboid cartilage. A model of the entire foot, containing bones, plantar soft tissue, and cartilage was generated (**Figure 9**).

In addition to converting the 2-D slices into 3-D stacked image models, we used PolyLines to determine



Figure 8.
Cartilage between first metatarsal and medial cuneiform.

the center of volume and the inertial matrix of each bone via the parallel axis theorem. The bones were assumed to be of homogeneous density. This resulted in an inertial matrix that was based solely on the geometry of the bones and not on the mass density. While this “inertial” matrix would be inadequate for kinetic analysis, it is sufficient for describing the shape of the foot based on the volume and geometry of the bones.

The eigenvectors of the inertial matrix established the principal axes of each bone (**Figure 10**). To remove the subjectivity associated with manual measurements on X-rays as well as the limits of 2-D projections of 3-D osseous geometry, we determined relative angles between bones from the principal axes. The talus and its associated joints are involved with frontal, sagittal, and transverse plane rotations within the foot, and the remainder of the foot often moves relative to the talus. There-

fore, the position of all bones of the foot was determined relative to the talus. For example, we determined the direction cosine matrix between the first metatarsal principal axes (a 3×3 matrix M in the global coordinate system) and the talar principal axes (a 3×3 matrix T in the global coordinate system) by multiplying T^T by M . Using established trigonometric relationships, we calculated an Euler angle description (z - y - x) from the direction cosine matrix. These three angles describe the rotation of the first metatarsal relative to the talus; the rotations are made about the moving reference frame of the first metatarsal. The first rotation is about the z -axis, the second rotation is about the y -axis, and the third rotation is about the x -axis. (Note that the principal axes are determined before the *TrueGrid* surface mesh generation and thus are not subject to the potential additional levels of error introduced in those steps.) This procedure was done for the following bones: first metatarsal, second metatarsal, calcaneus, navicular, and cuboid.



Figure 9.
Model of foot, containing bones, plantar soft tissue, and cartilage.

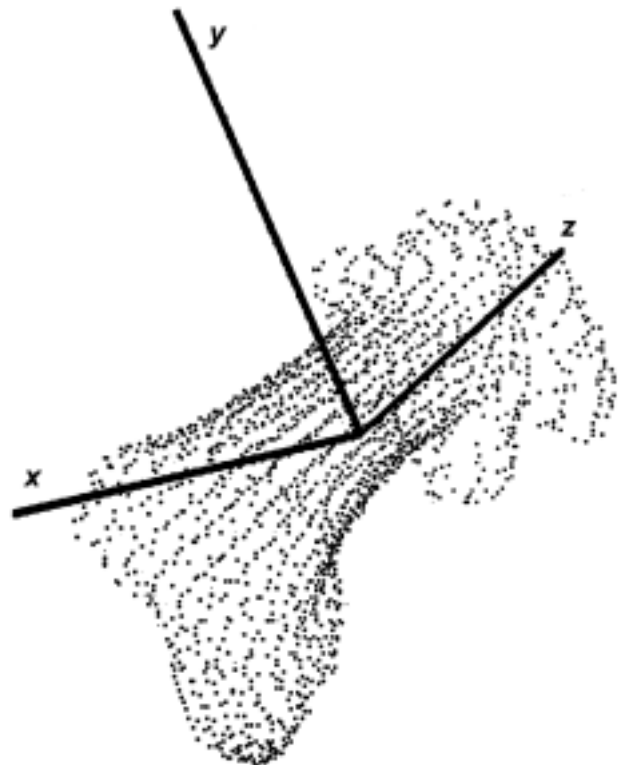


Figure 10.
Principal axes of first metatarsal.

RESULTS

We generated anatomically accurate representations of the osseous and soft tissues of the foot using the reconstruction algorithms. Data from CT images were processed for the generation of 3-D surface models of the bones, plantar soft tissue, and cartilage (Figures 4, 7, and 8). The individual bones of the foot that were developed separately were combined with the soft tissues into a model of the entire foot (Figure 9). Diagnostic analysis confirmed that the mesh quality was suitable for future finite element analysis.

The model provided objective, quantitative measures of the relative positions of the foot bones. We calculated the relative angles between bones from the principal axes for each bone (Figure 10). As an example, the three Euler angles (z - y - x) that describe the transformation from the first metatarsal to the talus are -89.6° , 8.4° , 15.6° (Figures 11 and 12). For each bone, the z -axis represents the axis about which the moment of inertia is smallest, the x -axis is the axis about which the moment of inertia is largest, and the y -axis is the cross product of the first two. The z -axis of the talus is the “long” axis, progressing from the center of mass anteriorly through the approximate center of the talar head. The y -axis is directed medially and the x -axis is directed superiorly. For the metatarsal, the z -axis is also the long axis, while the y -axis is directed dorsally and the x -axis directed

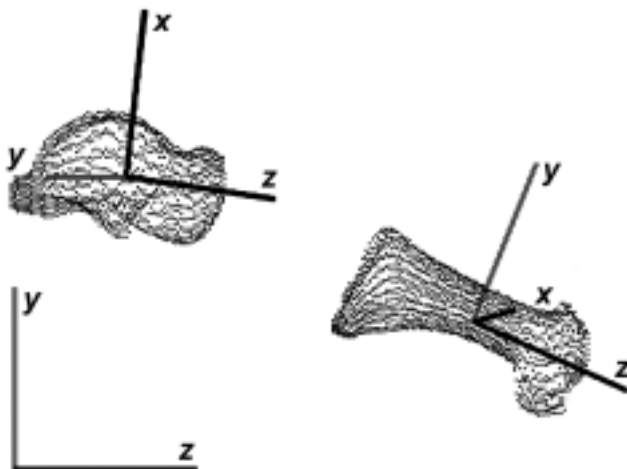


Figure 11. Sagittal plane relationship of principal axes of talus and first metatarsal.

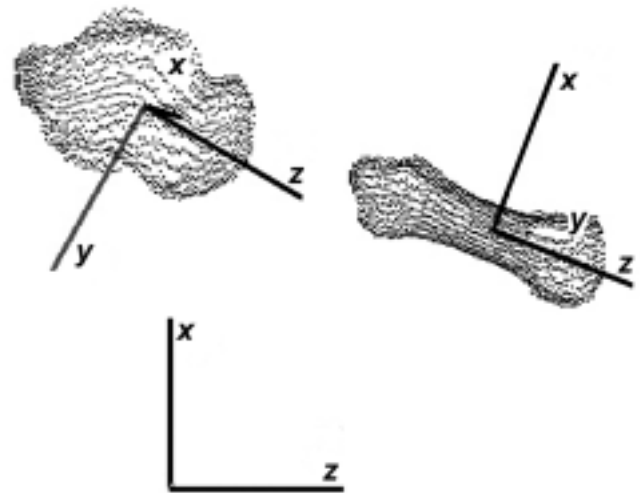


Figure 12. Transverse plane relationship of principal axes of talus and first metatarsal.

laterally. We also calculated relative angles between the talus and other foot bones as well (see Table).

Each relative angle describes a rotation of a bone about the talus; this relationship was determined for five bones, but we will discuss only the first metatarsal. For clarification, it may help to think of these two bones as they sit in the cardinal planes. The long or z -axes of both bones (about which there is less inertia) are directed approximately anteriorly. The x -axes (about which there is the greatest amount of inertia) are not similarly directed; the talar x -axis is directed superiorly, while the first metatarsal x -axis is directed laterally.

One can clarify the Euler angle description by picturing the two bones rotated so that their principal axes are coincident; from this position, the Euler angles describe the angular rotations that the first metatarsal must take relative to the talus to achieve its position in the cadaveric

Table.

Euler angle rotations describing the relationship between several bones of the foot and talus.

Bony Relationship	Alpha (z axis)	Beta (y axis)	Gamma (x axis)
First metatarsal to talus	-89.6	8.4	15.6
Second metatarsal to talus	-117.4	23.4	10.0
Calcaneus to talus	-71.6	34.3	-17.3
Navicular to talus	-134.4	-62.7	56.8
Cuboid to talus	-158.2	59.3	-21.2

specimen. A rotation of -89.6° about the z -axis describes a rotation of the first metatarsal about the long axis of the first metatarsal (which is coincident with the long axis of the talus at this point). Thus, the axes with the most inertia differ between the bones by almost 90° . The 8.55° rotation about the y -axis indicates that the first metatarsal is plantar flexed relative to the talus. The 15.50° rotation about the x -axis demonstrates an external rotation of the first metatarsal relative to the talus. These two rotations, describing roughly the sagittal and transverse plane relationships, are clinically relevant for the two bones in question.

DISCUSSION

Procedures for generating an anatomically detailed computer model from CT scans and for quantifying the relationships between the bones of the foot have been developed. Using custom software together with several commercial packages, we processed CT images so that surface models for individual bones, the plantar soft tissue, and cartilage were generated. These geometries were used to create a 3-D anatomically detailed foot model that will serve as the basis for a finite element foot model. For each individual bone, the principal axes were calculated from the inertial matrix. We used these axes, which were determined objectively, to determine the relative angles between bones; the angles describing the first metatarsal relative to the talus were presented as an example.

The study had several limitations. One important consideration was the amount of load applied to the foot while it was scanned. Because computer simulations typically start with unloaded initial conditions, scanning a minimally loaded specimen might be ideal for generating anatomical data for finite element modeling. However, when comparing the principal axes between different foot types, one should load specimens to physiological levels, because relative angles of foot bones will change when the foot is loaded. In the future, when additional feet from live subjects are studied and contrasted for differences, they will be loaded with an acrylic frame during data collection. However, for this paper, the unloaded protocol was sufficient for demonstrating the utility of the method.

Additionally, the geometry of the bodies representing the cartilage was not obtained from actual cartilage.

Instead, the cartilage models were created such that they filled the space between the bones. However, since the cartilage was not easy to distinguish in the CT images, our methodology provided the best geometrical representation possible within the limits of our system.

Certain steps in the reconstruction process did introduce limited amounts of subjective error. Although we attempted to quantify foot-bone position objectively, small amounts of subjectivity, e.g., the setting of the threshold level and the occasional need to perform manual pixel-level corrections with NIH Image, were impossible to avoid. However, the threshold level was constant for most CT images and the number of manual pixel-level corrections was minimal. Finally, while the single cadaveric foot specimen used in this study was thought to represent a typical adult foot and was deemed free of deformity or disease, the results discussed here do not represent a cross section of the population or the average results from a particular foot type.

The calculated relative angles between the talus and the first metatarsal provide information that is similar to the data obtained currently from planar radiographs. Two of the CT measurements, the plantar flexion and external rotation of the first metatarsal, describe angles that provide information similar to clinical X-ray measurements, i.e., the lateral talometatarsal angle and the transverse talometatarsal angle, respectively. However, the measurements were constructed in a different manner; i.e., the X-ray parameters were 2-D measurements made by one subjectively drawing lines connecting certain points on X-rays, while the CT parameters are 3-D measurements generated objectively from the osseous geometry. Thus, while a one-to-one correspondence between the parameters may not exist, both methods may describe similar trends for a particular foot type; e.g., flatfeet will have characteristic X-ray measurements as well as CT parameters between the first metatarsal and the talus. However, unlike the radiographic data, the CT data will provide an objective 3-D description of the relationship between bones.

The soft tissue and osseous mesh created in the current study provides a foundation for future finite element analysis of foot biomechanics. Generated with largely automated reconstruction algorithms, the mesh possesses anatomical details not described in previously mentioned existing foot models. These include more refined bones and plantar soft tissues, anatomically

accurate toes, and cartilage, all of which may be critical in accurately simulating foot behavior.

CONCLUSION

The methodology discussed in this paper lays the foundation for the development of a finite element model of the foot as well as for future work on quantifying differences in foot shape between different foot types. The 3-D shapes of the bones, cartilage, and plantar soft tissue obtained from the CT scans will provide the necessary anatomical detail to begin finite element foot modeling. The relative angles between bones, as calculated from the principal axes, allow for objective determination of the relationships between the bones of the foot. This will be a new way to quantify differences between foot types.

ACKNOWLEDGMENT

This research was supported by the Department of Veterans Affairs, Veterans Health Administration, Rehabilitation Research and Development Service, project number A0806C.

REFERENCES

- Morag E, Cavanagh PR. Structural and functional predictors of regional peak pressures under the foot during walking. *J Biomech* 1999;32(4):359–70.
- Meglan D. Enhanced analysis of human locomotion [PhD thesis]. Columbus: Ohio State University; 1991.
- Gilchrist LA. A computer simulation of human gait [PhD thesis]. Waterloo: University of Waterloo; 1994.
- Nakamura S, Crowninshield RD, Cooper RR. An analysis of soft tissue loading in the foot—a preliminary report. *Bull Prosthet Res* 1981;18(BPR 10–35)(1):27–34.
- Patil KM, Braak LH, Huson A. Stresses in a simplified two-dimensional model of the human foot—a preliminary analysis. *Mech Res Commun* 1993;1–7.
- Patil KM, Braak LH, Huson A. Analysis of stresses in two-dimensional models of normal and neuropathic feet. *Med Biol Eng Comput* 1996;34(4):280–84.
- Lemmon D, Shiang TY, Hashmi A, Ulbrecht JS, Cavanagh PR. The effect of insoles in therapeutic footwear: A finite element approach. *J Biomech* 1997;30(6):615–20.
- Ledoux WR, Hillstrom HJ. A graphics-based, anatomically detailed, forward dynamic simulation of the stance phase of gait, emphasizing the properties of the plantar soft tissue. 17th Congress of the International Society of Biomechanics; Calgary, Alberta; 1999. p. 110.
- Ledoux WR. A biomechanical model of the human foot with emphasis on the plantar soft tissue [PhD thesis]. Philadelphia: University of Pennsylvania; 1999.
- Saucerman JJ, Loppnow BW, Lemmon DR, Smoluk JR, Cavanagh PR. The effect of midsole plugs inserted into therapeutic footwear for localized plantar pressure relief. 24th Annual Meeting of the American Society of Biomechanics; Chicago (IL); 2000. p. 235–36.
- Beaugonin M, Haug E, Cesari D. Improvement of numerical ankle/foot model: Modeling of deformable bone. 41st Stapp Car Crash Conference; Orlando (FL); 1997. p. 225–37.
- Bedewi PG, Digges KH. Investigating ankle injury mechanisms in offset frontal collisions utilizing computer modeling and case-study data. 43rd Stapp Car Crash Conference; San Diego (CA); 1999. p. 185–202.
- Beillas P, Lavaste F, Nicolopoulos D, Kayventash K, Yang K, Robin S. Foot and ankle finite element modeling using CT-scan data. 43rd Stapp Car Crash Conference; San Diego (CA); 1999. p. 217–42.
- Dubbeldam R, Nilson G, Pal B, Eriksson N, Owen C, Roberts A, et al. A MADYMO model of the foot and leg for local impacts. 43rd Stapp Car Crash Conference; San Diego (CA); 1999. p. 185–202.
- Tannous RE, Bandak FA, Toridis TG, Eppinger RH. A three-dimensional finite element model of the human ankle: Development and preliminary application to axial impulsive loading. 40th Stapp Car Crash Conference; 1996; Albuquerque (NM); 1996. p. 219–38.
- Jacob S, Patil MK. Three-dimensional foot modeling and analysis of stresses in normal and early stage Hansen's disease with muscle paralysis. *J Rehabil Res Dev* 1999; 36(3):252–263.
- Staheli LT, Chew DE, Corbett M. The longitudinal arch: A survey of eight hundred and eighty-two feet in normal children and adults. *J Bone Joint Surg Am* 1987;69(3):426–28.
- Cavanagh PR, Rodgers MM. The arch index: A useful measure from footprints. *J Biomech* 1987;20(5):547–51.
- Hawes MR, Nachbauer W, Sovak D, Nigg BM. Footprint parameters as a measure of arch height. *Foot Ankle* 1992; 13(1):22–6.
- Chu WC, Lee SH, Chu W, Wang TJ, Lee MC. The use of arch index to characterize arch height: A digital image processing approach. *IEEE Trans Biomed Eng* 1995; 42(11):1088–93.
- Tareco JM, Miller NH, MacWilliams BA, Michelson JD. Defining flatfoot. *Foot Ankle Int* 1999;20(7):456–60.

22. Bordelon RL. Correction of hypermobile flatfoot in children by molded insert. *Foot Ankle* 1980;1(3):143–50.
23. Gould N. Graphing the adult foot and ankle. *Foot Ankle* 1982;2(4):213–19.
24. Allard P, Sirois JP, Thiry PS, Geoffroy G, Duhaime M. Roentgenographic study of cavus foot deformity in Friedreich ataxia patients: Preliminary report. *Can J Neurol Sci* 1982;9(2):113–17.
25. Sangeorzan BJ, Mosca V, Hansen ST Jr. Effect of calcaneal lengthening on relationships among the hindfoot, midfoot, and forefoot. *Foot Ankle* 1993;14(3):136–41.
26. Myerson MS, Corrigan J, Thompson F, Schon LC. Tendon transfer combined with calcaneal osteotomy for treatment of posterior tibial tendon insufficiency: A radiological investigation. *Foot Ankle Int* 1995;16(11):712–18.
27. Saltzman CL, Nawoczenski DA, Talbot KD. Measurement of the medial longitudinal arch. *Arch Phys Med Rehabil* 1995;76(1):45–49.
28. Dyal CM, Feder J, Deland JT, Thompson FM. Pes planus in patients with posterior tibial tendon insufficiency: Asymptomatic versus symptomatic foot. *Foot Ankle Int* 1997;18(2):85–88.
29. Chen YJ, Huang TJ, Hsu KY, Hsu RW, Chen CW. Subtalar distraction realignment arthrodesis with wedge bone grafting and lateral decompression for calcaneal malunion. *J Trauma* 1998;45(4):729–37.
30. Rose GK. Pes planus. In: Jahss MH, editor. *Disorders of the foot and ankle: medical and surgical management*. Philadelphia (PA): W. B. Saunders; 1982.
31. Welton EA. The Harris and Beath footprint: Interpretation and clinical value. *Foot Ankle* 1992;13(8):462–68.
32. Thomson CE. An investigation into the reliability of the valgus index and its validity as a clinical measurement. *Foot* 1994;4:191.
33. Song J, Hillstrom HJ, Secord D, Levitt J. Foot type biomechanics: A comparison of planus and rectus foot types. *J Am Podiatr Med Assoc* 1996;86(1):16–23.
34. Grasso A, Scarfi G. Computed tomography demonstration of calcaneal morphotypes in plantar arch abnormalities. *Radiol Med (Torino)* 1993;85(4):384–88.

Submitted for publication November 1, 2000. Accepted in revised for November 15, 2001.